Atmos. Chem. Phys. Discuss., 11, 31735–31767, 2011
www.atmos-chem-phys-discuss.net/11/31735/2011/
doi:10.5194/acpd-11-31735-2011

Atmospheric Chemistry and Physics Discussions

The impact of Great Basin Desert dust on the summer monsoon system over southwestern North America

C. Zhao, X. Liu, and L. R. Leung

Atmospheric Sciences and Global Change Division, Pacific Northwest National Laboratory, Richland, WA, USA

Received: 20 October 2011 – Accepted: 22 November 2011 – Published: 2 December 2011

Correspondence to: C. Zhao (chun.zhao@pnnl.gov)

Published by Copernicus Publications on behalf of the European Geosciences Union.

Abstract

The radiative forcing of dust emitted from the Great Basin Desert (GBD) and its impact on monsoon circulation and precipitation over the North America monsoon (NAM) region are simulated using a coupled meteorology and aerosol/chemistry model (WRF-Chem) for 15 yr (1995–2009). During the monsoon season, dust has a cooling effect ($-0.90\,W\,m^{-2}$) at the surface, a warming effect ($0.40\,W\,m^{-2}$) in the atmosphere, and a negative top-of-the-atmosphere (TOA) forcing ($-0.50\,W\,m^{-2}$) over the GBD region on 24-h average. Most of the dust emitted from the GBD concentrates below 800 hPa and stacks over the western slope of the Rocky Mountains and Mexican Plateau. The absorption of shortwave radiation by dust heats the lower atmosphere by up to $0.5\,K\,day^{-1}$ over the western slope of the Mountains. Model sensitivity simulations with and without dust for 15 summers (June-July-August) show that dust heating of the lower atmosphere over the GBD region remotely strengthens the low-level southerly moisture fluxes on both sides of the Sierra Madre Occidental. It also results in an eastward migration of NAM-driven moisture convergence over the western slope of the Mountains. These monsoonal circulation changes lead to a statistically significant increase of precipitation by up to ~40 % over the eastern slope of the Mountains (Arizona-New Mexico-Texas regions). This study highlights the interaction between dust and the NAM system and motivates further investigation of possible dust feedback on monsoon precipitation under climate change and the mega-drought conditions projected for the future.

1 Introduction

The North American Monsoon (NAM) system is a major climate system that significantly affects the regional hydrological cycle over large areas of the southwestern United States (US) and northwestern Mexico. The NAM system is characterized by a combination of seasonally warm land surfaces and atmospheric moisture from nearby

ACPD
11, 31735–31767, 2011

maritime sources that together produce convection that contributes over 70 % of annual precipitation to the region. The NAM summer rainfall typically begins in July with a pronounced increase from an extremely dry condition and lasts until September when the dry regime reestablishes (Adams and Comrie, 1997). The Great Basin Desert (GBD), the largest US desert, covers an arid expanse of ~190 000 square miles and is bordered by the Sierra Nevada Range on the west and the Rocky Mountains on the east, the Columbia Plateau to the north and the Mojave and Sonoran deserts to the south. The Great Basin Desert is north of the NAM region.

The Great Basin Desert is the main source of dust aerosol over the southwestern US. Dust aerosol has important climate impact through changes in solar and terrestrial radiation and radiative and microphysical properties of clouds (e.g. Sokolik et al., 1998; Ginoux et al., 2001; Lau et al., 2009; Zhao et al., 2011). The dust lofted from the deserts near the monsoon regions may affect monsoon circulation and precipitation worldwide. Recent years, many efforts have begun to study dust impacts on the West African Monsoon (WAM) and the Asian Monsoon (AM) circulation and precipitation, using general circulation models (GCMs) and regional models combined with observations (e.g. Miller et al., 2004; Yoshioka et al., 2007; Lau et al., 2006, 2009; Kim et al., 2010; Zhao et al., 2011). These studies have provided important understanding of the fundamental processes associated with dust effect on the two monsoon systems. Over West Africa, Lau et al. (2009) and Kim et al. (2010) showed that the Saharan dust radiative effect could strengthen the WAM, which is manifested in a northward shift of the West African precipitation over land. Kim et al. (2010) and Zhao et al. (2011) also found that dust could affect not only the total amount but also diurnal cycle of WAM precipitation simulated by a GCM and a regional model, respectively. Over Asia, Lau et al. (2006) elucidated a plausible "heat-pump" mechanism for dust impact on the Asian summer monsoon using the NASA finite-volume GCM. As dust from the deserts of western China, Pakistan, and the Middle East are transported into and stacked up against the northern and southern slopes of the Tibet Plateau, the dust heated air over the slopes can draw in warm and moist air over the Indian subcontinent, suggesting

ACPD
11, 31735–31767, 2011

that the dust loading may lead to an advance of the rainy periods and subsequently an intensification of the Indian summer monsoon.

Although the dust emitted from the Great Basin Desert over the Southwest US is less than that emitted from the Saharan desert and the deserts over Asia, the NAM system is also weaker than the monsoon systems over West Africa and Asia. Therefore, dust could still have significant effect on the NAM system. The IPCC AR4 climate model simulations projected warmer and dryer conditions for the southwestern US and northwestern Mexico in the 21st century. The projected drought parallels the severity of the 1930s Dust Bowl (Seager et al., 2007). The mega-droughts may lead to widespread dust storms (e.g. Woodhouse and Overpeck, 1998) that interact with the NAM system, strengthening or weakening the monsoon system through positive or negative feedbacks. To the best of our knowledge, the potential dust impact on NAM is not fully understood.

To improve understanding of dust impact on NAM in current and future climate conditions, as the first step, we used the regional model WRF-Chem to investigate the dust impact on the NAM system in the current climate condition. The objective of this study is to investigate the radiative forcing of GBD dust and how it affects the NAM circulation and precipitation at a regional scale. This study (1) examines both SW and LW radiative forcings of GBD dust during the NAM season over the Southwest US, and (2) investigates the potential dust effects on circulation and precipitation during the NAM season. Dust effects on cloud and precipitation through aerosol indirect effects are not considered in this study as the primary dust source region is generally removed from the monsoon core region where clouds are prominent (Sect. 4.1). The paper is organized as follows. Sections 2 and 3 detail the WRF-Chem model and the measurements used in this study. The SW and LW radiative forcings of the GBD dust and their impact on the NAM circulation and precipitation are analyzed in Sect. 4. The paper concludes in Sect. 5.

ACPD
11, 31735–31767, 2011

2 Model description

WRF-Chem, a version of WRF (Skamarock et al., 2008), simulates trace gases and particulates simultaneously with the meteorological fields (Grell et al., 2005). Grell et al. (2005) implemented the RADM2 (Regional Acid Deposition Model 2) photochemical mechanism (Stockwell et al., 1990) and the MADE/SORGAM (Modal Aerosol Dynamics Model for Europe (MADE) and Secondary Organic Aerosol Model (SORGAM)) aerosol model (Ackermann et al., 1998; Schell et al., 2001) into WRF-Chem. MADE/SORGAM in WRF-Chem uses the modal approach with three modes (Aitken, accumulation, and coarse modes, assuming a log-normal distribution within each mode) to represent the aerosol size distribution. Different aerosol species within each size mode are assumed to be internally mixed so that all particles within a size mode have the same chemical composition. In MADE/SORGAM, aerosol species include sulfate, nitrate, ammonium, black carbon (BC), organic matters (OM), sea salt, mineral dust, and water. Aerosol optical properties for scattering (e.g. single-scattering albedo, asymmetry factor, and extinction) are computed as a function of wavelength and three-dimensional position. A complex refraction index is calculated by volume averaging for each mode for each chemical constituent of the aerosol. To efficiently compute the extinction efficiency (Q_e) and the scattering efficiency (Q_s), WRF-Chem follows a methodology described by Ghan et al. (2001) that performs the full Mie calculations once first to obtain a table of seven sets of Chebyshev expansion coefficients, and later the full Mie calculations are skipped and Q_e and Q_s are calculated using bilinear interpolation over the Chebyshev coefficients stored in the table. A detailed description of the computation of aerosol optical properties in WRF-Chem can be found in Fast et al. (2006) and Barnard et al. (2010).

The version of WRF-Chem model with MADE/SORGAM coupled with GOCART dust scheme was first used by Zhao et al. (2010) to investigate the sensitivities in simulating the size distributions and optical properties of Saharan dust to emitted dust size distributions and aerosol size treatments during the dry season (from January to February)

ACPD
11, 31735–31767, 2011

of 2006 over West Africa. It was used by Zhao et al. (2011) to further understand the various radiative forcings of Saharan dust and how they jointly affect the hydrological cycle at a regional scale. In this study, the model domain covers the entire US and northern Mexico (133.05° W–58.95° W, 15.95° N–51.53° N) using 150 × 100 grid points at 36 km horizontal resolution and 35 vertical layers with model top pressure at 100 hPa. Two sets of 15-yr simulations are conducted from 10 April to 31 August for 1995–2009 with and without dust. Only the results from 1 June to 31 August each year (referred as the NAM season hereafter) are used in the analysis to minimize the impact from the chemical and land surface initial conditions. In addition, we only analyzed the simulated results from 140 × 90 interior points (129.0° W–62.0° W, 17.0° N–50.0° N) of the domain to minimize the influence from the lateral boundary conditions. The model configuration for dust simulation follows Zhao et al. (2010, 2011). The refractive index of dust is set to $1.53 + 0.003i$ as Zhao et al. (2010, 2011) over West Africa because of insufficient information to constrain the values over the Southwest US. The rapid radiative transfer model (RRTMG) (Mlawer et al., 1997; Iacono et al., 2000) for both SW and LW radiation is used to simulate aerosol direct radiative effect. The Morrison scheme and Grell scheme are used to represent cloud microphysics and convection processes. Although the aerosol activation to cloud droplet is included to account for cloud chemistry and aerosol wet deposition (Gustafson et al., 2007), dust indirect radiative effect on the NAM system is not investigated in this study, because the simulated dust coincides minimally with the NAM precipitation region and dust effect by acting as ice nuclei (IN) is not treated in the current version of WRF-Chem. The Noah land surface model and Mellor-Yamada-Janjic (MYJ) planetary boundary scheme are used.

Large-scale meteorological fields are assimilated with lateral boundary and initial conditions from the North American Regional Reanalysis (NARR) data, which also provide the prescribed sea surface temperature (SST) for the simulations. Chemical lateral boundary conditions are from the default profiles in WRF-Chem, which are based on the averages of mid-latitude aircraft profiles from several field studies over the eastern Pacific Ocean (McKeen et al., 2002). Anthropogenic emissions are obtained

ACPD
11, 31735–31767, 2011

from the US National Emission Inventory (NEI) 2005 (WRF-Chem user guide from http://ruc.noaa.gov/wrf/WG11/Users_guide.pdf). Biomass burning emissions are obtained from the Global Fire Emissions Database, Version 3 (GFEDv3) with monthly temporal resolution (van der Werf et al., 2010).

3 Observations

3.1 AERONET surface observation network

The Aerosol Robotic Network (AERONET) (Holben et al., 1998) has ~100 identical globally distributed sun- and sky-scanning ground-based automated radiometers, which provide measurements of aerosol optical properties throughout the world (Dubovik and King, 2000; Dubovik et al., 2002). In this study, AERONET measured aerosol optical depth (AOD) at 675 nm and 440 nm from one Arizona site (Maricopa, 111.97° W, 33.07° N, Fig. 1) near the dust source region are used to derive the AOD at 550 nm (using the Angström exponent) for comparison with model results. All of the retrievals of AOD are quality level 2, and the uncertainty of AOD measurements is about ±0.01 (Holben et al., 2001). In this study, the available data from 2003 to 2009 are used to evaluate the modeling results during the same period.

3.2 MODIS

The Moderate Resolution Imaging Spectroradiometer (MODIS) instruments with wide spectral range, high spatial resolution, and near daily global coverage are designed on board the NASA Aqua platforms to observe and monitor the Earth changes including tropospheric aerosols (Kaufman et al., 1997). The standard MODIS aerosol product does not retrieve aerosol information over bright surfaces (e.g. desert) due to a strong surface spectral contribution in the visible range (Kaufman et al., 1997). However, a new algorithm, called the "Deep Blue algorithm" (Hsu et al., 2006), has been integrated

ACPD
11, 31735–31767, 2011

with the existing MODIS algorithm to retrieve AOD even over bright surfaces. Therefore, the retrieved "deep blue" AOD from MODIS (Collection 5.1) (only available over land so far) (Levy et al., 2007; Remer et al., 2005) is used in this study. The MODIS on board the Aqua platform passes over the equator at ~13:30 LT during daytime (Kaufman et al., 1997). In this study, the available data from 2003 to 2009 are used to evaluate the modeling results during the same period. Model results are sampled in the same overpass time as Aqua when comparing with MODIS retrievals.

3.3 MISR

Since February 2000, the Multi-angle Imaging SpectroRadiometer (MISR) instrument on board the NASA Terra platform observes AOD continuously at nine distinct zenith angles, ranging from 70° afterward to 70° forward, and in four narrow spectral bands centered at 446, 558, 672, and 866 nm. MISR's unique blend of directional and spectral data allows aerosol retrieval algorithms to be used that do not depend on the explicit radiometric surface properties. Therefore, MISR can retrieve aerosol properties even over highly reflective surfaces (e.g. deserts) (Diner et al, 1998; Martonchik et al., 2004). The MISR on board the Terra platform passes over the equator at ~10:45 LT during daytime (Diner et al, 2001). In this study, the available data from 2003 to 2009 are used to evaluate the modeling results during the same period. Model results are sampled in the same overpass time as Terra when comparing with MISR retrievals.

3.4 IMPROVE

The Interagency Monitoring for Protected Visual Environments (IMPROVE) program was started in 1985 by the US federal agencies EPA, National Park Services, Department of Agriculture-Forest Service, and other land management agencies as a part of the EPA Regional Haze program (Malm et al., 1994). There are more than 100 IMPROVE sites in the US regularly measuring aerosol chemical compositions as well as fine and coarse mode aerosol mass concentrations (http://vista.cira.colostate.edu/

ACPD
11, 31735–31767, 2011

IMPROVE). The mass of dust is estimated from the measured elements associated predominantly with soil, including Ti, Al, Si, Ca, and Fe. The uncertainties of estimated values results from the range and variation of mineral composition from a variety of soil types (see Malm et al., 1994 for details). Since there is no IMPROVE sites over the GBD, fine dust (with diameter less than 2.5 µm) mass concentrations from the 7 sites in the region (110° W–112° W, 31° N–35° N, mostly locate in the Arizona state, Fig. 1) near the GBD during 1995–2009 are used to evaluate model results.

3.5 TRMM

The 3B-43 product of the Tropical Rainfall Measuring Mission (TRMM) data is used. The purpose of algorithm 3B-43 is to produce TRMM merged high quality (HQ)/infrared (IR) precipitation and root-mean-square (RMS) precipitation-error estimates. These gridded estimates are on a monthly temporal resolution and a 0.25 × 0.25 degree spatial resolution in a global belt extending from 50° S to 50° N latitude. Detailed description of the dataset can be found in Huffman et al. (2001, 2007). In this study, the available data from 2000 to 2009 are used to evaluate the modeling results during the same period.

3.6 PERSIANN

Precipitation Estimation from Remote Sensing Information using Artificial Neural Network (PERSIANN) provides hourly precipitation data on a 0.25 × 0.25 degree spatial resolution in a global belt extending from 60° S to 60° N latitude (Hsu et al., 1999; Sorooshian et al., 2000). In the PERSIANN system, a neural network trained by precipitation from the TRMM Microwave Imager (TMI) and other microwave measurements (Hsu et al., 1997, 1999) was used to estimate 30-min precipitation rates from infrared (IR) and visible imagery from geostationary satellites. In this study, the available data from 2000 to 2009 are used to evaluate the modeling results during the same period.

ACPD
11, 31735–31767, 2011

4 Results and discussion

4.1 Modeling GBD dust and its radiative forcing

Figure 1 shows the monthly mean spatial distribution of 10-m wind circulation from NARR reanalysis data and WRF-Chem simulations in June, July, August, and summer averaged for 1995–2009. The dust emissions from WRF-Chem simulations are also shown. In general, the model well captures the surface wind circulation compared to the NARR reanalysis data. Dust emission occurs mostly over the southwestern US. The monthly variation of dust emission is small during summer. WRF-Chem simulates a total dust emission of 2.4 Tg for the summer season. Figure 2 shows the monthly mean spatial distribution of wind circulation at 800 hPa from NARR reanalysis data and WRF-Chem simulations in June, July, August, and summer averaged for 1995–2009. The dust mass concentration at 800 hPa from WRF-Chem simulations is also shown. The model simulated wind circulation is consistent with the reanalysis data. In general, dust concentrates near the GBD region in all months. The model simulates higher dust concentration over the source region in July and August than that in June. The dust in June stretches further east than that in July and August.

The model simulated surface mass concentration of fine dust (with diameter <2.5 µm) is compared to the IMPROVE data at the sites near the dust source region (Fig. 3). The daily variation of dust concentration at the sites from both model simulations and IMPROVE data is small. The 15-yr summer average of dust concentrations at all sites from model simulations is 2.2 µg m^{-3}, well consistent with the IMPROVE data of 2.0 µg m^{-3}. The simulated AOD near the dust source region is also evaluated with the AERONET, MODIS, and MISR measurements at the AERONET site Maricopa. The model simulates 7-yr summer mean AOD of 0.14 at site Maricopa, which is close to the AERONET measured value of 0.16 and the MISR retrieved value of 0.17. MODIS retrieved a much higher value of 0.40. Compared to the AOD value of 0.09 from the sensitivity model simulations without dust emissions, the dust contributes ~40 % of AOD at the site Maricopa.

ACPD
11, 31735–31767, 2011

Figure 4 shows the WRF-Chem simulated 24-h averaged spatial distribution of clear-sky dust SW, LW, and net (SW + LW) radiative forcing at the top and bottom of the atmosphere and in the atmosphere during the summer period over North America. The dust radiative forcing is derived from the WRF-Chem simulations with and without dust. At the top of atmosphere (TOA), the dust SW radiative forcing is negative throughout the domain. The pattern is consistent with the spatial distribution of dust mass concentration (Fig. 2) with the highest forcing of $-1.25\,W\,m^{-2}$ over the desert region. The dust LW radiative forcing at TOA is mostly close to zero with some slightly positive values over the domain. Overall, the simulated dust net (SW+LW) radiative forcing at TOA has a cooling effect of $-0.1\,W\,m^{-2}$ on domain average with a maximum of $-1.15\,W\,m^{-2}$ over the GBD. In the atmosphere, dust absorbs SW and warms the atmosphere. Dust LW effect cools the atmosphere. The dust LW forcing is higher over the desert because of the hotter desert surface and stronger interaction between LW and coarse mode dust particles that are spatially confined to the desert due to their shorter lifetimes and distance being carried. In the atmosphere, dust produces a net (LW + SW) warming effect with a domain average of $0.05\,W\,m^{-2}$ and a maximum of $0.6\,W\,m^{-2}$. At the surface, dust has a cooling effect (domain average of $-0.2\,W\,m^{-2}$ and maximum of $-2.1\,W\,m^{-2}$) by reducing the downward SW radiation and a warming effect (domain average of $0.05\,W\,m^{-2}$ and maximum of $0.98\,W\,m^{-2}$) by trapping the LW radiation emitted from surface. The net (LW + SW) dust radiative forcing at the surface is $-0.15\,W\,m^{-2}$ on domain average and $-1.38\,W\,m^{-2}$ on maximum. Over the GBD region, the dust has a cooling effect ($-0.90\,W\,m^{-2}$) at the surface, a warming effect ($0.40\,W\,m^{-2}$) in the atmosphere, and a negative TOA forcing ($-0.50\,W\,m^{-2}$).

4.2 Radiative impact of GBD dust on NAM precipitation and circulation

4.2.1 NAM precipitation and circulation

Figure 5a shows the monthly and seasonal mean spatial distribution of precipitation from TRMM and PERSIANN observations and WRF-Chem simulations over North

ACPD
11, 31735–31767, 2011

America. Both TRMM and PERSIANN show a typical monthly monsoonal evolution. Monsoon onset occurs in June in most of western Mexico south of ~30° N and reaches the international border and then the southwestern US in July and August. Rainfall intensifies strongly and rapidly in July, with maximum rainfall rates along the western foothills of the Sierra Madre Occidental in northwestern Mexico, consistent with previous studies (e.g. Gutzler, 2009). Although, TRMM observes the spatial variability of the NAM precipitation, it underestimates the NAM precipitation compared to the PERSIANN data. It has been found that TRMM has low biases for NAM precipitation (Gutzler, 2009). The model successfully simulates the observed spatial distribution of the monthly monsoonal evolution with the northward migration of the rain-belt. The model reproduces the monsoonal precipitation maximum across northwest Mexico. To further investigate the NAM feature, the NAM region is defined in the black box (20° N–40° N, 120° W–95° W) following previous studies (Gutzler, 2004, 2009).

Figure 5b shows the monthly and seasonal mean spatial distribution of precipitation over the NAM region from the WRF-Chem simulations. It has been stated that the NA monsoon is most visible in Arizona and New Mexico states of the US and the northwest of Mexico (Adams and Comire, 1997). Four sub-regions (black boxes) are further defined for time series analysis within the NAM region: DESERT, CORE, AZNM, and TXNM. The DESERT region is defined to cover the dust source region with a very low precipitation (<10 mm month^{-1}). The CORE region is defined to cover the tongue of the NAM rain-belt that receives the highest precipitation among the four sub-regions. The AZNM region is defined as the region over Arizona and New Mexico, which are the two states that are most affected by the NAM in the southwestern US and receive ~50 % of their annual precipitation during the NAM season (Adams and Comrie, 1997). The TXNM region is defined adjacent to the east of the CORE and AZNM regions.

To examine lower tropospheric moisture transports in the NAM region, longitude-height cross-section of zonal and meridional moisture fluxes are investigated. Figure 6 shows the WRF-Chem simulated monthly mean cross-section of zonal circulation and meridional moisture fluxes at 29° N from 115° W to 105° W (Fig. 5a) during the NAM

ACPD
11, 31735–31767, 2011

season, extending across the Gulf of California onto the high topography of the Sierra Madre Occidental. At 29° N, the Gulf of California extends zonally between 113° W and 111° W. The model correctly resolves the low level southerly jet along the western foothills of the Sierra Madre Occidental, extending from surface to 900 hPa. The model clearly exhibits a monthly-mean southerly moisture fluxes maximum near 111° W in the vicinity of Gulf of California. The low-level southerly moisture fluxes increase from 10 g kg^{-1} m s^{-1} to 50 g kg^{-1} m s^{-1} from June to August. On the other side, the eastern slopes of the Sierra Madre Occidental, the model also simulates the near-surface southerly moisture fluxes from Gulf of Mexico. Corresponding to the two southerly jets confined to the lower atmosphere, the model also simulates a northerly moist jet at 700–800 hPa at ~109° W near the top of the Sierra Madre Occidental. Besides the meridional jets, the zonal moisture fluxes show a convergence at the western slope of the Sierra Madre Occidental, which is consistent with the maximum NAM precipitation over the region. The convergence is stronger in July–August than June.

4.2.2 Dust impact on precipitation and circulation

Figure 7 shows the monthly precipitation and dust-induced change over the three NAM sub-regions (CORE, AZNM, and TXNM) from WRF-Chem simulations during May–August averaged for 1995–2009. The dust-induced precipitation change is calculated by subtracting the results from the WRF-Chem simulations without dust from the results from the WRF-Chem simulations with dust. In general, the WRF-Chem simulations without dust show that precipitation increases from ~40 mm month^{-1} to ~200 mm month^{-1} over the CORE region and from ~24 mm month^{-1} to ~65 mm month^{-1} over the AZNM region during May–August corresponding to the NAM northward migration, while the precipitation over the TXNM region reduces from ~56 mm month^{-1} to ~40 mm month^{-1}.

The dust-induced precipitation change mainly occurs in July and August over all three regions. Over the CORE region, dust increases precipitation by 3 mm month^{-1} (1 %) in July and 12 mm month^{-1} (6 %) in August. Over the AZNM region, dust

ACPD
11, 31735–31767, 2011

increases precipitation by 6 mm month^{-1} (12 %) in July and 3 mm month^{-1} (6 %) in August. Over the TXNM region, dust increases precipitation by 12 mm month^{-1} (25 %) in July and 15 mm month^{-1} (40 %) in August. Although the monthly variation of precipitation over the TXNM region corresponds least with the NAM migration, the dust-induced precipitation change increases most significantly along with the NAM migration. From the spatial distribution of dust-induced precipitation, statistically significant impact of dust is mainly found within the AZNM and TXNM regions (not shown). The dust-induced precipitation change over the two regions exceeds the 90 % statistical significance level based on the Student's t-test.

Dust affects precipitation mainly through changes in the surface energy budget and atmospheric diabatic heating profiles via direct radiative forcing and changes in cloud property via semi-direct and indirect radiative forcing. Locally, dust aerosol cools the surface and warms the atmosphere during daytime, hence increases atmospheric stability (e.g. Zhao et al., 2011). However, over the NAM region, since most of the dust concentrates over the DESERT region, the dust direct radiative forcing over the three sub-regions (CORE, AZNM, and TXNM) is relatively small (Fig. 4). In addition, dust semi-direct and indirect effect is also limited over the three sub-regions because dust is mostly confined to its source region and there is no treatment of dust as ice nuclei (IN) in our simulations. However, the heated air by dust over the DESERT region could remotely affect the overall monsoonal circulations (e.g. Lau et al, 2006, 2009).

Figure 8 shows the monthly mean cross sections of dust-induced change of zonal and meridional moisture fluxes at 29° N from 115° W to 105° W during the NAM season averaged for 1995–2009. Same as Fig. 7, the dust-induced circulation change is calculated by subtracting the results from the WRF-Chem simulations without dust from the results from the WRF-Chem simulations with dust. In general, the dust impact on the moisture transport is negligible in June, but it becomes significant in July and August. In July and August, the southerly moisture fluxes are strengthened by 1–6 g kg^{-1} m s^{-1} (~10 %) on both western and eastern slopes of the Sierra Madre Occidental. In the meantime, the easterly moisture fluxes are also strengthened by the

ACPD
11, 31735–31767, 2011

GBD dust-induced heating, particularly in August, resulting in a shift of moisture convergence to the east of the Sierra Madre Occidental. Overall, the GBD dust helps to draw in warm and moist air from the Gulfs of California and Mexico, resulting in a general increase in NAM precipitation over all three sub-regions.

The TXNM region is taken as an example to further illustrate the correlation between dust-induced diabatic heating and the NAM precipitation change. Figure 9 shows the monthly daytime dust-induced diabatic heating change over the DESERT region along with the dust-induced precipitation change over the TXNM region for May–August, 1995–2009 from the WRF-Chem simulations. In May, dust-induced atmospheric diabatic heating over the DESERT region is small. It increases significantly from 0.05 K day^{-1} to 0.5 K day^{-1} from May to July–August. The dust heating effect reaches a maximum in July. Corresponding to the dust heating in the lower atmosphere (below 800 hPa), the dust-induced precipitation change over the TXNM region gradually increases from June to July when dust heating in the lower atmosphere over the DESERT region is largest.

5 Summary and conclusions

In this study, the radiative forcing of GBD dust and its feedback to the monsoon precipitation and circulation over the NAM region are investigated using the WRF-Chem model. To establish statistical significance of dust effects, simulation results for May–August of 1995–2009 are analyzed to capture potential dominant dust effects above interannual variability. Both dust SW and LW direct radiative effect are included. Generally, the model simulates reasonable aerosol mass concentrations and optical depth over the NAM region during summer. Compared to the observations, the model successfully reproduces the magnitude and spatial distribution of NAM precipitation.

The WRF-Chem simulates a total GBD dust emission of 2.4 Tg during the NAM season. The GBD dust concentrates near the source region in the lower atmosphere (below 800 hPa) during summer, resulting in negative TOA forcing by up to −1.25 W m^{-2}

ACPD
11, 31735–31767, 2011

over the source region. In the atmosphere, the GBD dust absorbs SW and warms the atmosphere by 0.05 W m^{-2} on domain average and up to 0.6 W m^{-2} over the source region. At the surface, the GBD dust has a cooling effect of −0.15 W m^{-2} on domain average and −1.38 W m^{-2} on maximum over the source region. Overall, the net (LW + SW) radiative effect of GBD dust is atmospheric warming, surface cooling, and negative TOA forcing over North America.

The WRF-Chem successfully simulates the observed spatial distribution of the monthly monsoonal evolution with the northward migration of the rain-belt and properly resolves the low level southerly jet along the western foothills of the Sierra Madre Occidental, extending from the surface to 900 hPa. The GBD dust affects the NAM precipitation mostly over three NAM sub-regions: CORE, AZNM, and TXNM in July and August. Dust increases precipitation by 3 mm month^{-1} (1 %), 6 mm month^{-1} (12 %), and 12 mm month^{-1} (25 %) in July and 12 mm month^{-1} (6 %), 3 mm month^{-1} (6 %), and 15 mm month^{-1} (40 %) in August over the CORE, AZNM, and TXNM regions, respectively. The dust-induced precipitation change over the AZNM and TXNM regions exceeds the 90 % statistical significance level based on the Student's t-test.

The dust-induced precipitation change is facilitated by the dust-heated air over the DESERT region that helps to draw warm and moist air from the Gulfs of California and Mexico. In July and August, the southerly moisture fluxes at lower atmosphere are strengthened by ∼10 % on both western and eastern slopes of the Sierra Madre Occidental. In the meantime, the easterly moisture fluxes are also strengthened, resulting in an eastward shift of moisture convergence, leading to the largest precipitation increase in the TXNM region. The dust-induced precipitation changes are highly correlated with the dust-induced lower atmospheric (below 800 hPa) diabatic heating (up to 0.5 K day^{-1} in July and August) over the DESERT region. This mechanism of remote impact of dust on the overall monsoonal circulations is similar as that proposed by Lau et al. (2006, 2009) over Asia and West Africa.

Compared to the previous studies on the Saharan dust impact on the West Africa Monsoon (WAM) system (e.g. Lau et al. 2009), the GBD dust plays a similar role as a

ACPD
11, 31735–31767, 2011

"heat pump" to strengthen the monsoon circulation and re-distributes the precipitation. Although the GBD dust forcing over the southwestern US is much smaller than the Saharan dust over West Africa, it still has a significant impact on the NAM circulation and precipitation, because the diabatic heating that drives the NAM is also much smaller than that of WAM. For example, residual diagnosis of NAM diabatic heating based on two global reanalysis data suggests a maximum averaged low level heating no more than 1.5 K day^{-1} in the Sierra Madre Occidental (Barlow et al., 1998) (1–2 K day^{-1} at 700 hPa simulated in this study). Therefore the dust heating of 0.5 K day^{-1} estimated from our simulations could produce significant effects on the NAM circulation depending on its location and vertical distribution. However, the diurnal cycle of NAM precipitation is not changed significantly by the GBD dust, which is different from the role of Saharan dust found by previous studies (e.g. Kim et al., 2010; Zhao et al., 2011). The negligible GBD dust impact on the diurnal cycle of NAM precipitation is related to the low dust concentration and therefore negligible impact on atmospheric stability over the precipitation region. Overall, this study highlights the interaction between the GBD dust and NAM system and motivates further investigation of possible dust feedback on the monsoon under climate change and the projected mega-drought conditions over the southwestern US in the 21st century.

Finally, several caveats should be noted in this study. First, in the absence of measurements of GBD dust optical property, this study uses the same refractive index of dust as our previous studies over West Africa (Zhao et al., 2010, 2011). The imaginary part of dust refractive index is uncertain (e.g. Balkanski et al., 2007; McConnell et al., 2010; Zhao et al., 2011) and may change the dust-induced atmospheric diabatic heating, which triggers the NAM circulation and precipitation change. In order to constrain the GBD dust absorption, measurements of the GBD dust optical properties are required in the future. Second, although the dust impact on diabatic heating and hence the NAM circulation is evident, the dust-induced changes of NAM precipitation may be sensitive to the cloud microphysics and convective schemes used in the model, which is beyond the scope of this study. We note, however, that the simulations reported

ACPD
11, 31735–31767, 2011

in this study reproduced the seasonal cycle and spatial distribution of NAM precipitation rather well, hence lending some confidence in simulated response to changes in dust diabatic heating. Third, although the GBD dust-induced atmospheric heating influences the NAM circulation and precipitation, the effect cannot be fully simulated using a regional modeling framework because the same SST lower boundary conditions and atmospheric lateral boundary conditions are used in the simulations with and without dust. However, this limitation may not have large impacts because the GBD dust is rather spatially confined so its impacts on large-scale circulation may not extend well beyond the boundaries of our simulation domain. On the other hand, NAM precipitation is generally not well simulated by GCM's because higher spatial resolution is needed to represent the complex landscape and its interactions with regional and large-scale circulation over the NAM region. Last, dust indirect effects on convective cloud and precipitation are not represented in the current convective microphysical parameterization, although convective precipitation dominates during the NAM season (generating over 90 % of precipitation in the simulations). In addition, the dust aerosol cannot be activated as ice nuclei (IN) to influence clouds in the Morrison microphysics scheme in this study. Despite the low occurrence of dust over the NAM cloud/precipitation region, episodic intrusions of dust to the CORE region due to anomalous transport could result in important aerosol indirect effects that deserve further study in the future.

Acknowledgements. This study is supported by the Department of Energy Earth System Modeling Program Investigations on the Magnitude and Probabilities of Abrupt Climate TransitionS (IMPACTS) project. This research used computing resources from the National Energy Research Scientific Computing Center, which is supported by the Office of Science of the US Department of Energy under Contract No. DE-AC02-05CH11231. Pacific Northwest National Laboratory is operated for the US DOE by Battelle Memorial Institute under contract DE-AC06-76RLO330 1830.

ACPD
11, 31735–31767, 2011

References

Ackermann, I. J., Hass, H., Memmesheimer, M., Ebel, A., Binkowski, F. S., and Shankar, U.: Modal aerosol dynamics model for Europe: Development and first applications, Atmos. Environ., 32, 2981–2999, 1998.

Adams, D. and Comrie, A. C.: The North American Monsoon, B. Am. Meteorol. Soc., 78, 2197–2213, 1997.

Balkanski, Y., Schulz, M., Claquin, T., and Guibert, S.: Reevaluation of Mineral aerosol radiative forcings suggests a better agreement with satellite and AERONET data, Atmos. Chem. Phys., 7, 81–95, doi:10.5194/acp-7-81-2007, 2007.

Barlow, M., Nigam, S., and Berbery, E. H.: Evolution of the North American Monsoon System, J. Clim., 11, 2238–2257, 1998.

Barnard, J. C., Fast, J. D., Paredes-Miranda, G., Arnott, W. P., and Laskin, A.: Technical Note: Evaluation of the WRF-Chem "Aerosol Chemical to Aerosol Optical Properties" Module using data from the MILAGRO campaign, Atmos. Chem. Phys., 10, 7325–7340, doi:10.5194/acp-10-7325-2010, 2010.

Diner, D. J., Beckert, J., Reilly, T., Bruegge, C., Conel, J., Kahn, R., Martonchik, J., Ackerman, T., Davies, R., Gerstl, S., Gordon, H., Muller, J., Myneni, R., Sellers, P. J., Pinty, B., and Verstraete, M.: Multi-angle Imaging SpectroRadiometer (MISR) instrument description and experiment overview, IEEE T. Geosci. Remote, 36, 1072–1087, 1998.

Diner, D. J., Abdou, W. A., Bruegge, C. J., Conel, J. E., Crean, K. A., Gaitley, B. J., Helmlinger, M. C., Kahn, R. A., Martonchik, J. V., and Pilorz, S. H.: MISR aerosol optical depth retrievals over southern Africa during the SAFARI-2000 dry season campaign, Geophys. Res. Lett., 28, 3127–3130, 2001.

Dubovik, O. and King, M. D.: A flexible inversion algorithm for retrieval of aerosol optical properties from sun and sky radiance measurements, J. Geophys. Res., 105, 20673–20696, 2000.

Dubovik, O., Holben, B., Eck, T. F., Smirnov, A., Kaufman, Y. J., King, M. D., Tanre, D., and Slutsker, I.: Variability of absorption and optical properties of key aerosol types observed in worldwide locations, J. Atmos. Sci., 59, 590–608, 2002.

Fast, J. D, Gustafson Jr., W. I., Easter, R. C., Zaveri, R. A., Barnard, J. C., Chapman, E. G., and Grell, G. A.: Evolution of ozone, particulates, and aerosol direct forcing in an urban area using a new fully-coupled meteorology, chemistry, and aerosol model, J. Geophys. Res., 111, D21305, doi:10.1029/2005JD006721, 2006.

ACPD
11, 31735–31767, 2011

Fast, J., Aiken, A. C., Allan, J., Alexander, L., Campos, T., Canagaratna, M. R., Chapman, E., DeCarlo, P. F., de Foy, B., Gaffney, J., de Gouw, J., Doran, J. C., Emmons, L., Hodzic, A., Herndon, S. C., Huey, G., Jayne, J. T., Jimenez, J. L., Kleinman, L., Kuster, W., Marley, N., Russell, L., Ochoa, C., Onasch, T. B., Pekour, M., Song, C., Ulbrich, I. M., Warneke, C., Welsh-Bon, D., Wiedinmyer, C., Worsnop, D. R., Yu, X.-Y., and Zaveri, R.: Evaluating simulated primary anthropogenic and biomass burning organic aerosols during MILAGRO: implications for assessing treatments of secondary organic aerosols, Atmos. Chem. Phys., 9, 6191–6215, doi:10.5194/acp-9-6191-2009, 2009.

Ghan, S., Laulainen, N., Easter, R., Wagener, R., Nemesure, S., Chapman, E., Zhang, Y., and Leung, R.: Evaluation of aerosol direct radiative forcing in MIRAGE, J. Geophys. Res., 106, 5295–5316, 2001.

Ginoux, P., Chin, M., Tegen, I., Prospero, J. M., Holben, B., Dubovik, O., and Lin, S.: Sources and distributions of dust aerosols simulated with the GOCART model, J. Geophys. Res., 106, 20225–20273, 2001.

Grell, G. A., Peckham, S. E., Schmitz, R., and McKeen, S. A., Frost, G., Skamarock, W. C., and Eder, B.: Fully coupled "online" chemistry within the WRF model, Atmos. Environ., 39, 6957–6976, 2005.

Gustafson, W. I., Chapman, E. G., Ghan, S. J., Easter, R. C., and Fast, J. D.: Impact on modeled cloud characteristics due to simplified treatment of uniform cloud condensation nuclei during NEAQS 2004, Geophys. Res. Lett., 34, L19809, doi:10.10.1029/2007GL030021, 2007.

Gutzler, D. S. et al.: North American monsoon Model Assessment Project (NAMAP). NCEP/Climate Prediction Center Atlas No. 11, 32 pp, available online at: http://www.cpc.ncep.noaa.gov/research_papers/ncep_cpc_atlas/11/atlas11.htm, 2004.

Gutzler, D. S., Long, L. N., Schemm, J., Baidya Roy, S., Bosilovich, M., Collier, J. C., Kanamitsu, M., Kelly, P., Lawrence, D., Lee, M., Sanchez, R., Mapes, B., Mo, K., Nunes, A., Ritchie, E., Roads, J., Schubert, S., Wei, H., and Zhang, G.: Simulations of the 2004 North American Monsoon: NAMAP2, J. Climate, 22, 6716–6740, doi:10.1175/2009JCLI3138.1, 2009.

Holben, B. N., Eck, T. F., Slutsker, I., Tanr' e, D., Buis, J. P., Stezer, A., Vermote, E., Reagan, Y., Kaufman, U. J., Nakajima, T., Lavenu, F., Jankowiak, I., and Smirnov, A.: AERONET-A federated instrument network and data archive for aerosol characterization, Remote Sens. Environ., 66, 1–16, 1998.

Holben, B. N., Tanre, D., Smirnov, A., ECK T. F., Slutsker, I., Abuhassan, N., Newcomb, W., Schafer, J., Chatenet, B., Lavenu, F., Kaufman, Y., Vande Castle, J., Setzer, A., Markham,

ACPD
11, 31735–31767, 2011

B., Clark, D., Frouin, R., Halthore, R., Karneli, A., O'Neill, N., Pietras, C., Pinker, R., Voss, K., and Zibordi, G.: An emerging ground-based aerosol climatology: Aerosol optical depth from AERONET, J. Geophys. Res., 106, 12067–12097, 2001.

Hsu, K., Gao, X., Sorooshian, S., and Gupta, H. V.: Precipitation estimation from remotely sensed information using artificial neural networks., J. Appl. Meteor., 36, 1176–1190, 1997.

Hsu, K., Gupta, H., Gao, X., and Sorooshian, S.: Estimation of physical variables from multi-channel remotely sensed imagery using a neural network: application to rainfall estimation., Water Resour. Res., 35, 1605–1618, 1999.

Hsu, N. C., Tsay, S., King, M., and Herman, J. R.: Deep blue retrievals of Asian Aerosol Properties during ACE-Asia, IEEE T. Geosci. Remote Sens., 44, 3180, doi:10.1109/TGRS.2006.879540, 2006.

Huffman, G. J., Adler, R. F., Morrissey, M., Bolvin, D. T., Curtis, S., Joyce, R., McGavock, B., and Susskind, J.: Global Precipitation at One-Degree Daily Resolution from Multi-Satellite Observations, J. Hydrometeor., 2, 36–50, 2001.

Huffman, G. J., Adler, R. F., Bolvin, D. T., Gu, G., Nelkin, E. J., Bowman, K. P., Hong, Y., Stocker, E. F., and Wolff, D. B.: The TRMM Multi-satellite Precipitation Analysis: Quasi-Global, Multi-Year, Combined-Sensor Precipitation Estimates at Fine Scale, J. Hydrometeor., 8, 38–55, 2007.

Iacono, M. J., Mlawer, E. J., Clough, S. A., and Morcrette, J.-J.: Impact of an improved longwave radiation model, RRTM. on the energy budget and thermodynamic properties of the NCAR community climate mode, CCM3, J. Geophys. Res., 105, 14873–14890, 2000.

Kaufman, Y. J., Tanre, D., Remer, L. A., Vermote, E. F., Chu, A., and Holben, B. N.: Operational remote sensing of tropospheric aerosol over land from EOS moderate resolution imaging spectroradiometer, J. Geophys. Res., 102, 17051–17067, 1997.

Kim, K.-M., Lau, W. K.-M., Sud, Y. C., and Walker, G. K.: Influence of aerosol-radiative forcings on the diurnal and seasonal cycles of rainfall over West Africa and Eastern Atlantic Ocean using GCM simulations, Clim. Dyn., 35, 115–126, doi:10.1007/s00382-010-0750-1, 2010.

Lau, K. M., Kim, K. M., Sud, Y. C., and Walker, G. K.: A GCM study of the response of the atmospheric water cycle of West Africa and the Atlantic to Saharan dust radiative forcing, Ann. Geophys., 27, 4023–4037, doi:10.5194/angeo-27-4023-2009, 2009.

Levy, R. C., Remer, L. A., Tanre, D., Kaufman, Y. J., Ichoku, C., Holben, B. N., Livingston, J. M., Russell, P. B., and Maring, H.: Evaluation of the Moderate-Resolution Imaging Spectro-radiometer (MODIS) retrievals of dust aerosol over the ocean during PRIDE, J. Geophys.

ACPD
11, 31735–31767, 2011

Res., 108, D198594, doi:10.1029/2002JD002460, 2003.
Malm, W., Sisler, J., Huffman, D., Eldred, R., and Cahill, T.: Spatial and seasonal trends in particle concentration and optical extinction in the United States, J. Geophys. Res., 99, 1347–1370, 1994.
Martonchik, J. V., Diner, D. J., Kahn, R., and Gaitley, B.: Comparison of MISR and AERONET aerosol optical depths over desert sites, Geophys. Res. Lett., 31, L16102, doi:10.1029/2004GL019807, 2004.
McConnell, C. L., Formenti, P., Highwood, E. J., and Harrison, M. A. J.: Using aircraft measurements to determine the refractive index of Saharan dust during the DODO Experiments, Atmos. Chem. Phys., 10, 3081–3098, doi:10.5194/acp-10-3081-2010, 2010.
McKeen, S. A., Wotawa, G., Parrish, D. D., Holloway, J. S., Buhr, M. P., Hubler, G., Fehsenfeld, F. C., and Meagher, J. F.: Ozone production from Canadian wildfires during June and July of 1995, J. Geophys. Res., 107, 4192, doi:10.1029/2001JD000697, 2002.
Miller, R. L., Tegen, I., and Perlwitz, J.: Surface radiative forcing by soil dust aerosols and the hydrologic cycle, J. Geophys. Res., 109, D04203, doi:10.1029/2003JD004085, 2004.
Mlawer, E. J., Taubman, S. J., Brown, P. D., Iacono, M. J., and Clough, S. A.: RRTM, a validated correlated-k model for the longwave, J. Geophys. Res., 102, 16663–16682, 1997.
Remer, L. A., Kaufman, Y. J., Tanre, D., Mattoo, S., Chu, D. A., Martins, J. V., Li, R., Ichoku, C., Levy, R. C., Kleidman, R. G., Eck, T. F., Vermote, E., and Holben, B. N.: The MODIS aerosol algorithm, products and validation, J. Atmos. Sci., 62, 947–973, 2005.
Schell, B., Ackermann, I. J., Hass, H., Binkowski, F. S., and Ebel, A.: Modeling the formation of secondary organic aerosol within a comprehensive air quality modeling system, J. Geophys. Res., 106, 28275–28293, 2001.
Seager, R., Ting, M., Held, I., Kushnir, Y., Lu, J., Vecchi, G., Huang, H., Harnik, N., Leetmaa, A., Lau, N., Li, C., Velez, J., and Naik, N.: Model Projections of an Imminent Transition to a More Arid Climate in Southwestern North America, Science, 316, 1181–1184, doi:10.1126/science.1139601, 2007.
Skamarock, W. C., Klemp, J. B., Dudhia, J., Gill, D. O., Barker, D. M., Duda, M. G., Huang, X., Wang, W., and Powers, J. G.: A description of the advanced research WRF version 3, NCAR Tech. Note, NCAR/TN-475+STR, 8 pp., Natl. Cent. for Atmos. Res., Boulder, Colo, available at: http://www.mmm.ucar.edu/wrf/users/docs/arw_v3.pdf, 2008
Sokolik, I. N., Toon, O. B., and Bergstrom, R. W.: Modelling the radiative characteristics of air-airborne mineral aerosols at infrared wavelengths, J. Geophys. Res., 103, 8813–8826,

ACPD
11, 31735–31767, 2011

1998.
Sorooshian, S., Hsu, K., Gao, X., Gupta, H., Imam, B., and Braithwaite, D.: Evaluation of PERSIANN system satellite-based estimates of tropical rainfall., B. Am. Meteorol. Soc., 81, 2035–2046, 2000.
Stockwell, W. R., Middleton, P., Chang, J. S., and Tang, X.: The second generation regional acid deposition model chemical mechanism for regional air quality modeling, J. Geophys. Res., 95, 16343–16367, 1990.
van der Werf, G. R., Randerson, J. T., Giglio, L., Collatz, G. J., Mu, M., Kasibhatla, P. S., Morton, D. C., DeFries, R. S., Jin, Y., and van Leeuwen, T. T.: Global fire emissions and the contribution of deforestation, savanna, forest, agricultural, and peat fires (1997–2009), Atmos. Chem. Phys., 10, 11707–11735, doi:10.5194/acp-10-11707-2010, 2010.
Woodhouse, C. A. and Overpeck, J. T.: 2000 Years of Drought Variability in the Central United States, B. Am. Meteo. Soc., 79, 2693–2714, 1998.
Yoshioka, M., Mahowald, N., Conley, A. J., Collins, W. D., Fillmore, D. W., Zender, C. S., and Coleman, D. B.: Impact of desert dust radiative forcing on Sahel precipitation: relative importance of dust compared to sea surface temperature variations, vegetation changes and greenhouse gas warming, J. Climate, 16, 1445–1467, doi:10.1175/JCLI4056.1, 2007.
Zaveri, R. A. and Peters, L. K.: A new lumped structure photochemical mechanism for large-scale applications, J. Geophys. Res., 104, 30387–30415, 1999.
Zaveri, R. A., Easter, R. C., Fast, J. D., and Peters, L. K.: Model for simulating aerosol interactions and chemistry (MOSAIC), J. Geophys. Res., 113, D13204, doi:10.1029/2007JD008792, 2008.
Zhao, C., Liu, X., Leung, L. R., Johnson, B., McFarlane, S. A., Gustafson Jr., W. I., Fast, J. D., and Easter, R.: The spatial distribution of mineral dust and its shortwave radiative forcing over North Africa: modeling sensitivities to dust emissions and aerosol size treatments, Atmos. Chem. Phys., 10, 8821–8838, doi:10.5194/acp-10-8821-2010, 2010.
Zhao, C., Liu, X., Ruby Leung, L., and Hagos, S.: Radiative impact of mineral dust on monsoon precipitation variability over West Africa, Atmos. Chem. Phys., 11, 1879–1893, doi:10.5194/acp-11-1879-2011, 2011.

ACPD
11, 31735–31767, 2011

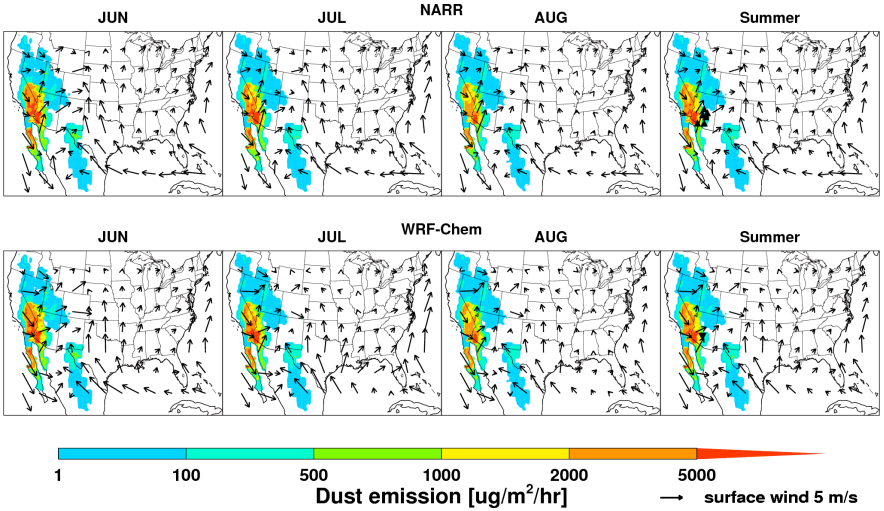

Fig. 1. Spatial distributions of 10-m wind from NARR reanalysis data and WRF-Chem simulations and dust emissions from WRF-Chem simulations in June, July, August, and summer averaged for 1995–2009. The seven upward black triangles (rightmost of the top panel) represent the IMPROVE sites; the one downward black triangle (rightmost of the bottom panel) represents the AERONET site Maricopa in Arizona.

ACPD
11, 31735–31767, 2011

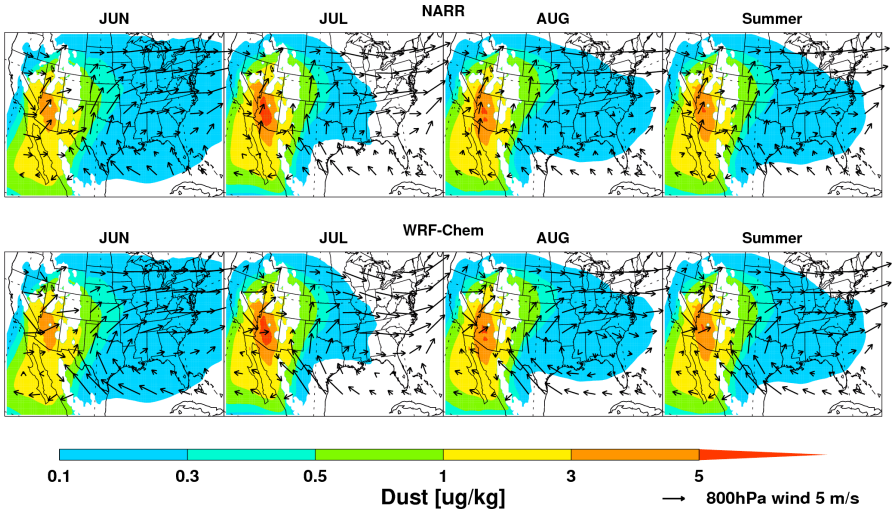

Fig. 2. Spatial distributions of wind from NARR reanalysis data and WRF-Chem simulations and dust concentrations from WRF-Chem simulations at 800 hPa in June, July, August, and summer averaged for 1995–2009.

ACPD
11, 31735–31767, 2011

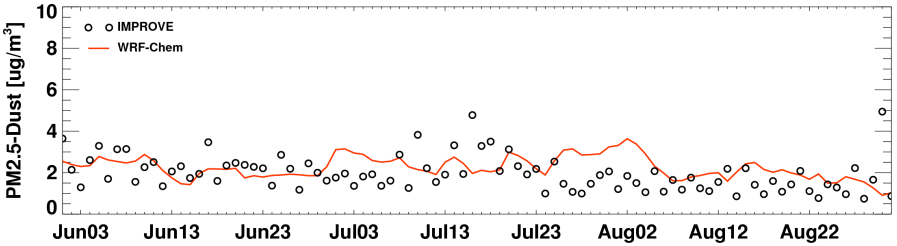

Fig. 3. Daily fine dust (with diameter <2.5 µm) mass concentrations averaged for the seven IMPROVE sites (Fig. 1) over the southwestern US from the IMPROVE measurements and WRF-Chem simulations for June–August, 1995–2009.

ACPD
11, 31735–31767, 2011

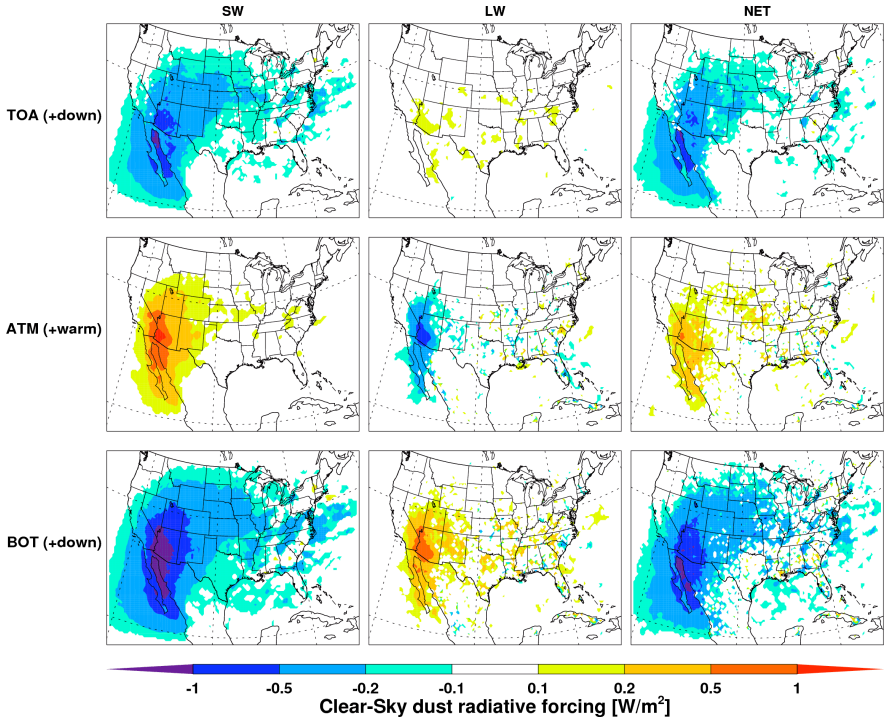

Fig. 4. Averaged clear-sky SW and LW radiative forcing of GBD dust over North America from WRF-Chem simulations. "TOA (+down)" represents the dust radiative forcing at the top of atmosphere and positive refers to downward direction; "ATM (+warm)" represents the dust radiative forcing in the atmosphere and positive refers to warming effect; "BOT (+down)" represents the dust radiative forcing at the surface and positive refers to downward direction. "Net" represents the sum of dust SW and LW radiative forcing.

ACPD
11, 31735–31767, 2011

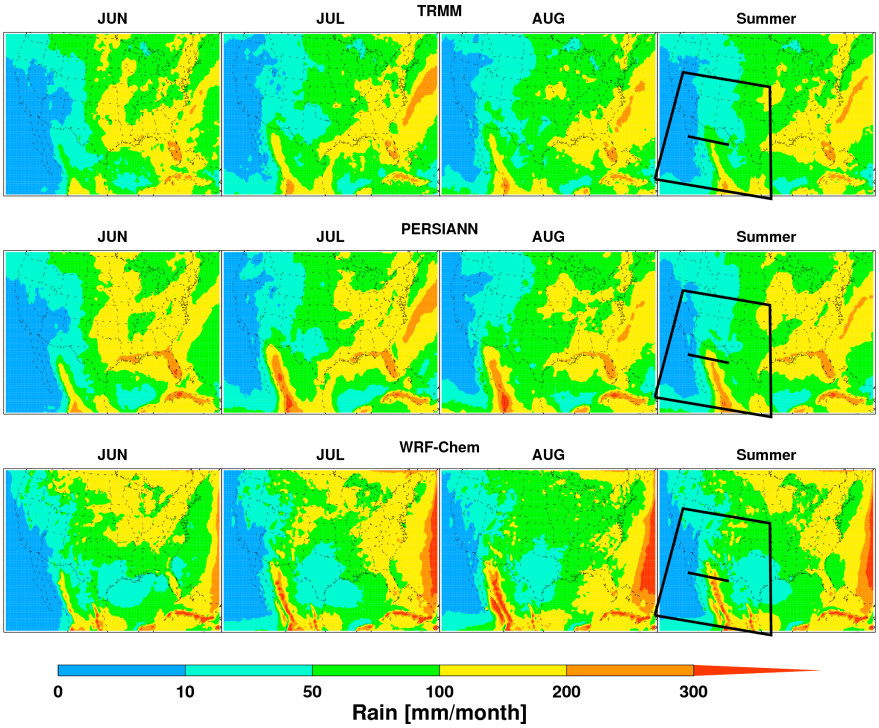

Fig. 5a. Spatial distributions of precipitation from TRMM and PERSIANN data and WRF-Chem simulations in June, July, August, and summer averaged for 2000–2009. The region in black box is defined as the North America Monsoon (NAM) region (20° N–40° N, 120° W–95° W). The black line within the black box represents the cross section at 29° N from 115° W to 105° W.

ACPD
11, 31735–31767, 2011

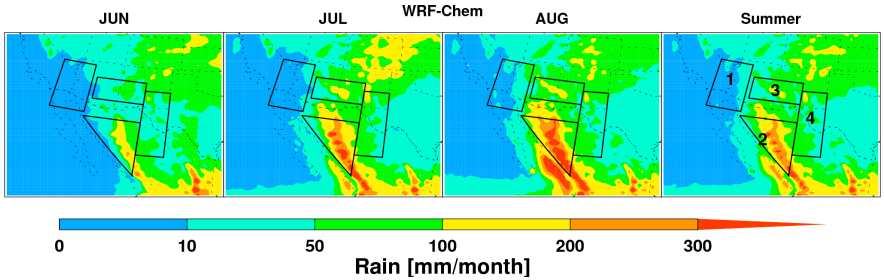

Fig. 5b. Spatial distributions of precipitation over the NAM region from WRF-Chem simulations in June, July, August, and summer averaged for 1995–2009. Four sub-regions are defined in the black boxes: Region 1 (DESERT), Region 2 (CORE), Region 3 (AZNM), and Region 4 (TXNM).

ACPD
11, 31735–31767, 2011

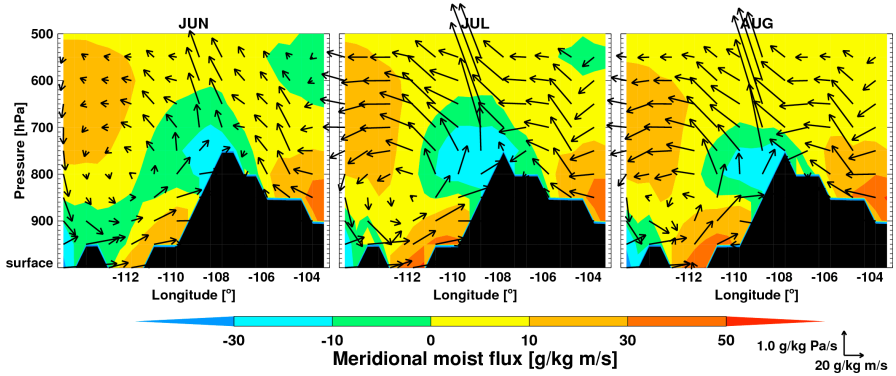

Fig. 6. Monthly mean cross sections of zonal circulation and meridional moisture fluxes at 29° N from 115° W to 105° W (Fig. 5a) during the NAM season. The color contour shows the meridional moisture fluxes. The positive values represent southerlies and negative values represent northerlies.

ACPD
11, 31735–31767, 2011

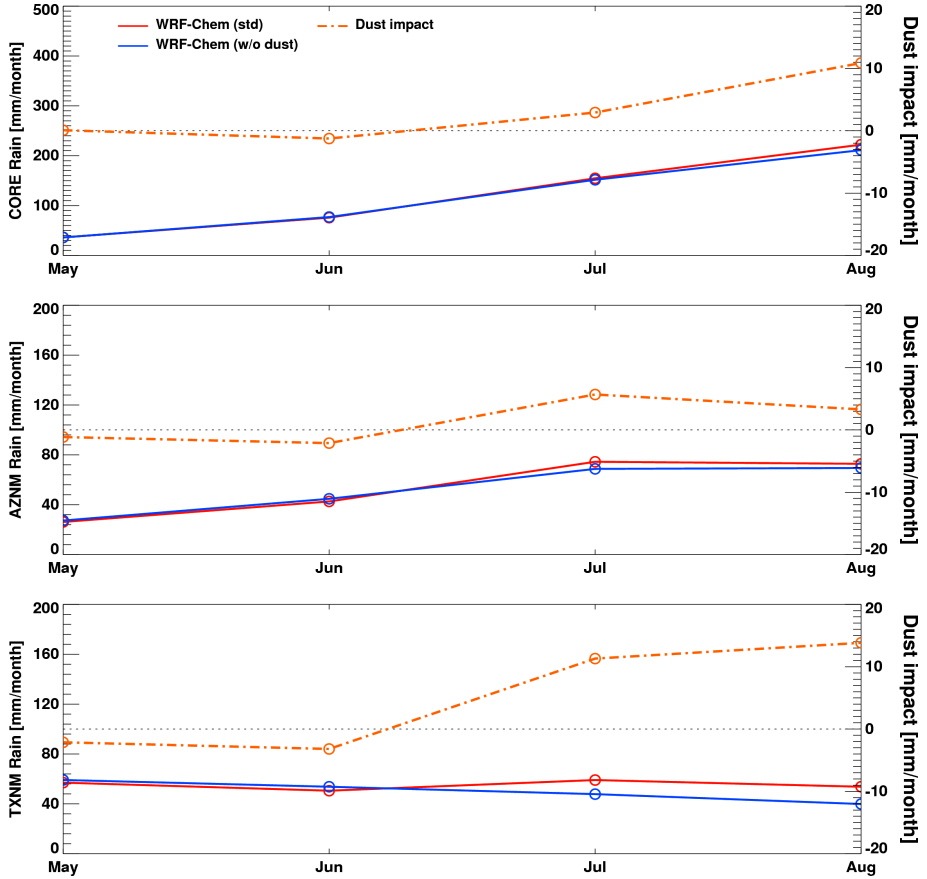

Fig. 7. Monthly precipitation and dust-induced change averaged over the three NAM sub-regions (CORE, AZNM, and TXNM) from the WRF-Chem simulations for May–August, 1995–2009.

ACPD
11, 31735–31767, 2011

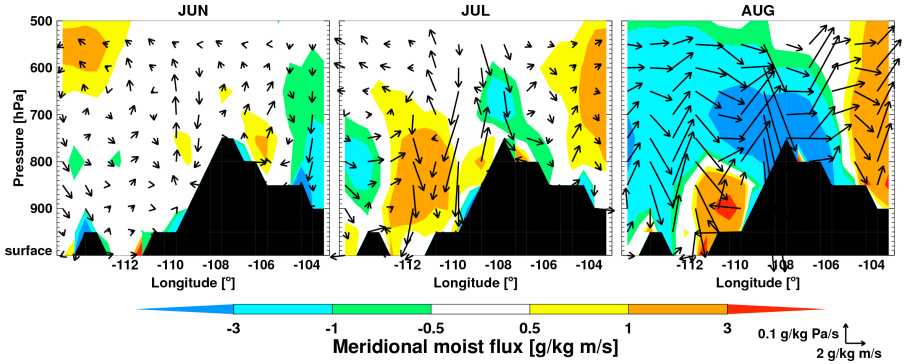

Fig. 8. Monthly mean cross sections of dust-induced change of zonal and meridional moisture fluxes at 29° N from 115° W to 105° W during the NAM season. The color contour shows the change in meridional moisture fluxes. The positive values represent increase in southerlies and negative values represent increase in northerlies.

ACPD
11, 31735–31767, 2011

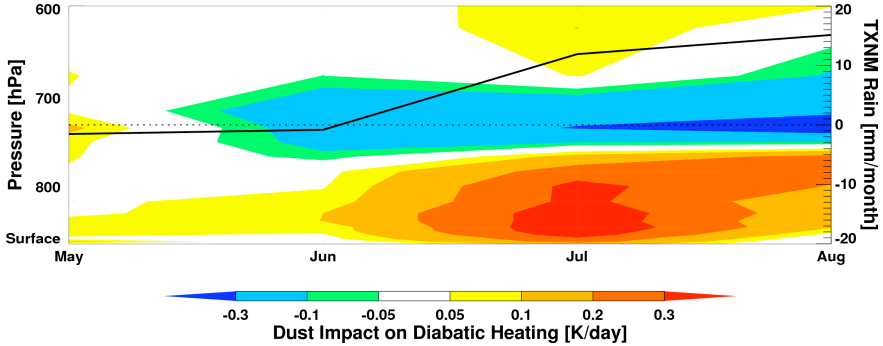

Fig. 9. Monthly dust-induced daytime diabatic heating change over the DESERT region along with the dust-induced precipitation change over the TXNM region from the WRF-Chem simulations for May–August, 1995–2009.

ACPD
11, 31735–31767, 2011